IDENTIFICATION OF FAILURE MODES IN SAFETY RELATED NUCLEAR STRUCTURES FOR MISSILE IMPACT

Neha Trivedi, R. K. Singh
Reactor Safety Division, Bhabha Atomic Research Centre, Trombay, Mumbai, INDIA-400085
E-mail of corresponding author: nehat@barc.gov.in

ABSTRACT

The impact induced failures in RC depends on the stiffness and mass ratio of the impactor and target, the pulse duration and drop height. Besides there are complexities due to concrete heterogeneity, inelastic response in different regimes and strain rate sensitivity. The paper evolves a transient dynamic finite element analysis procedure for reinforced concrete slabs subjected to hammer impact for explaining the observed crushing, cracking, flexural, punching shear and mixed failures based on fracture energy model. The numerical simulation of reinforced concrete slab impacted with cylindrical drop hammer as reported in experiment by Zineddin and Krauthammer [1] was carried out using ABAQUS/Explicit finite element code to explain various failure modes. It is shown that the realistic impact behavior of reinforced concrete slabs can be simulated through the present numerical procedure, which accounts for the fracture energy based softening model with due consideration to the above failure modes. It is illustrated that the failure modes can be numerically predicted through identifiable parameters such as the point of inflection and stress based criteria.

INTRODUCTION

The safety of some important structures such as nuclear containments, industrial buildings and underground facilities is an important concern. Impact loading on reinforced concrete structure such as due to aircraft crash, missile hit or free fall of a heavy machine part may cause different types of global or local damage such as flexure, penetration, scabbing, spalling, perforation and punching shear failure. The identification of each of the above failure modes is highly complex from the point of view of experiments as well as numerical simulations. To accurately analyze the structural response and the failure modes due to transient dynamic loads, it thus becomes necessary to develop a three-dimensional finite element model, which takes into account different types of material and geometrical nonlinearities. The prediction of failure modes for reinforced concrete structures under impulsive loads is a complex subject due to the effect of excitation of the higher modes of vibration, change in failure modes because of propagating stress waves, and a number of other failure mechanisms. The higher modes of vibration causes reverse reaction, reverse bending and localized high shear stress in addition to the generation of inflection point which consequently cause punching shear failure to be more dominant. During the last few decades numerous studies have been carried out to understand the behavior of reinforced concrete structures subjected to impact loading.

Zineddin and Krauthammer [1] studied experimentally the behavior of concrete slabs under impact loading. Reinforced concrete slab of size 90 mm × 1524 mm × 3353 mm (3.54 in x 60 in x 132 in) were hit by an advanced drop hammer device of 2608 kg (5750 lb) dropped from three predetermined heights of 152 mm (6 in), 305 (12 in) mm and 610 mm (24 in) respectively at the centre of the slab. The orthogonal layer of high strength reinforcement having 9.5 mm (0.37 in) diameter at 152 mm (6 in) c/c spacing was placed. The failure modes, deflection, and acceleration of slab were obtained. The result indicated that the response of slab is affected by amount of reinforcement and the variation in drop height.

The behavior of concrete is quite complex due to heterogeneity of material and various observed failure modes namely flexure, penetration, scabbing, spalling, perforation, direct and punching shear. The impact load induced failure of reinforced concrete structure needs to be understood with regard to the phenomenological composite models of concrete and steel members based on the observed failure modes at macroscopic level for a successful concrete slab design. Among the various inelastic models for reinforced concrete structure modeling, the limiting strain criteria was used conventionally, which is known to suffer from the limitation of mesh sensitivity. This has been addressed for static problems by Bazant et al [2] and fracture energy softening models have been suggested as remedial measures. Singh et al [3] have carried out a systematic numerical comparison of cohesive crack model and Bazant's crack band model to obtain mesh insensitive results as compared to the results obtained from limiting strain model. In this paper a comparative study is presented for the impact analysis of reinforced concrete slabs with limiting strain and fracture energy models with regard to the observed failure modes.

ANALYTICAL INVESTIGATION OF THREE-DIMENSIOANL RC SLAB

Finite Element Model, Loading and Boundary Conditions

Three dimensional model of the experimentally tested reinforced concrete slab by Zineddin and Krauthammer [1] was made using ABAQUS/CAE [4]. A one fourth quadrant of slab with over all dimensions of 3.496 m x 1.672 m (137.64 in x 65.83 in) span and 90 mm (3.54 in) thickness is modeled due to symmetry. The solid slab is modeled as three dimensional deformable body and the reinforcement as a three dimensional deformable wire shape element. The finite element mesh and the quadrant model of reinforced concrete slab having two steel-meshes of reinforcement is shown in Fig. 1 (a) & (b) respectively. The contact between the concrete and reinforcement was modeled using constraint in ABAQUS/CAE [4]. The concrete slab is taken as the host element and the reinforcement as embedded element. Meshing of concrete slab was done with 3D continuum elements (C3D8R) using the reduced integration and reinforcement is meshed as linear truss element (T3D2).

Impact loading is modeled as a time dependent pressure loading over the diameter of 250 mm (9.84 in) at the centre of slab for the peak loads of 304 KN (68.36 kip), 374 KN (84.09 kip) and 539 KN (121.1 kip) in case of A-2 mesh, B-2 mesh & C-2 mesh respectively with two steel-meshes in the slab. For the single steel-mesh, the peak loads are 228 KN (51.34 kip), 374 KN (84.09 kip) and 553 KN (124.2 kip) for A-1 mesh, B-1 mesh & C-1 mesh respectively. The pressure loadings for the above mentioned cases are obtained by distributing the peak load over the area of the impacted diameter. The load time history available in the study of Zineddin and Krauthammer [1] is simplified by enveloping the experimental time-amplitude curve in the present numerical study. The three dimensional slab is supported at the edges by providing fully constrained boundary conditions along the three axes and the boundary condition is given as u=0, v=0, w=0 with u, v & w as the displacements in x, y & z directions respectively. The v=0 on the x symmetric plane and u=0 on the y symmetric plane is applied to analyze a single quadrant of the slab.

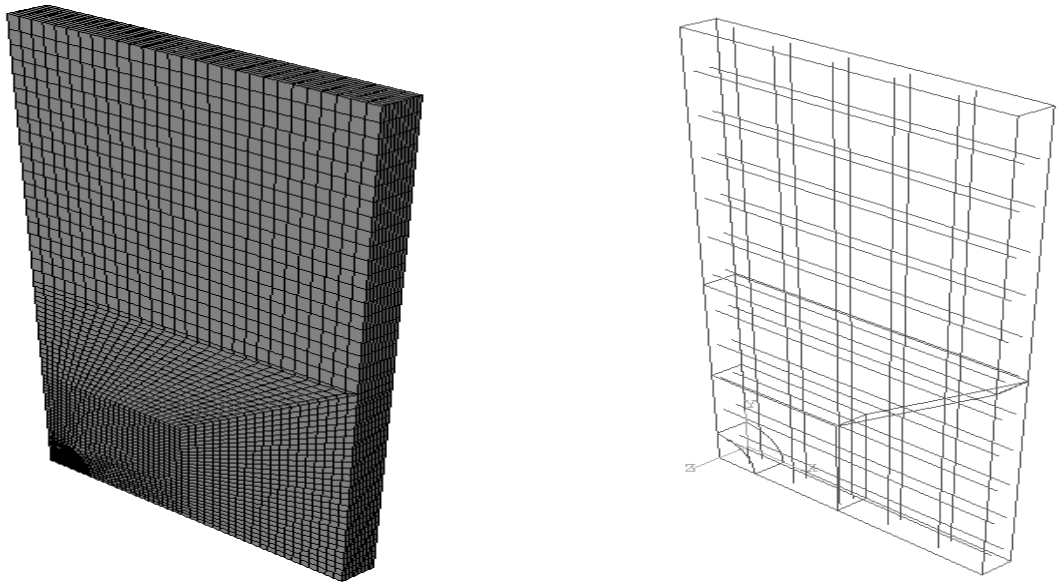

(a) (b)

Fig. 1 (a) Finite Element Mesh (b) RC slab with double reinforcement

Constitutive modeling

The material behavior of reinforced concrete slab is incorporated using the damage plasticity model that is capable of modeling quasi brittle material like concrete and the rebar by using conventional biaxial stress-strain plasticity model. It consists of plasticity and damage elasticity to describe the irreversible damage that occurs during the concrete fracturing process. The continuum plasticity-based damage model for concrete is based on the main two failure mechanisms, namely the tensile cracking and compressive crushing of the concrete material. The

compressive behavior of concrete is defined through stress strain curve of concrete by entering the yield stress and inelastic strain in ABAQUS/Explicit. The post-failure behavior is modeled with tension stiffening, for which the strain-softening behavior for cracked concrete is needed. The tension softening of concrete is defined by the scalar damage variable d. The concrete damaged plasticity model assumes a specified reduction of the elastic modulus and is given in terms of a scalar degradation variable *d* as:

$$E = (1-d) \times E_0 \quad (1)$$

Where d is the damage variable and E_0 is the static modulus of elasticity of concrete.

The tensile behavior of concrete in damaged plasticity model is defined by two ways; as Post-failure stress-strain relation and fracture energy cracking criteria. The concrete cracking strain, yield tensile strength of concrete and the damage parameters are defined for post failure stress strain relation approach. The cracking strain is expressed in the following form as given;

$$\varepsilon_t^{ck} = \varepsilon_t - \varepsilon_{0t}^{el} \quad (2)$$

Where ε_t is the total strain and ε_{0t}^{el} corresponds to the elastic strain of undamaged material. Fracture energy cracking criteria is associated with the energy required to open a unit area of crack. With this approach the concrete cracking behavior is characterized by a stress-displacement response rather than a stress-strain response. Under tension the concrete specimen cracks across some section. The damage parameter, fracture energy, cracking displacement and yield tensile strength of concrete is to be defined. The cracking displacement at which complete loss of strength takes place is expressed in the following form;

$$u_{to} = 2G_f / f_t^{'} \quad (3)$$

Where G_f is the fracture energy of concrete calculated through CEB-FIP model given by Mehta and Monteiro [5] and $f_t^{'}$ is the yield tensile strength of concrete.

The material constitutive parameters for concrete and steel are given in Table 1 and Table 2 respectively.

Table 1- Material parameters for concrete

Modulus of elasticity, E, N/m^2(ksi)	3.1e10(4495)
Poison's ratio, ν	0.17
Density, ρ (kg/m^3)	2400
Compressive strength, f_c',MPa (ksi)	37.5(5.44)
Tensile strength, f_t, MPa (ksi)	3.125(0.45)
Fracture energy, G_f, N/m(kip/inch)	90(5.14e-4)
Damage parameter, d	0.9
Cracking displacement, u_0,met (in)	5.76e-5(.0022)
Cracking strain	0.002

Table 2- Material parameters for steel

Modulus of elasticity, E, N/m^2(psi)	2e11(29000)
Poison's ratio, ν	0.33
Density, ρ(kg/m^3)	7850
Yield strength, f_t,MPa (ksi)	500 (72.5)
Strain Hardening, H,MPa (ksi)	2000 (290)

Investigation of Strain Rate Effect for the Slab Hammer Impact Problem

At the high strain rates up to 1000 s^{-1}, the apparent strength of concrete increases significantly. The dynamic increase factor (DIF), which is the ratio of the dynamic to static strength, is normally reported as the function of strain rate. Knowledge of the DIF is of significant importance in the design and analysis of structures for impact and shock loads. For concrete, the DIF can be more than two in compression, and more than six in tension at high strain rates. Strain-rate data for both the compressive and tensile strength of concrete is obtained from the study of Tedesco et.al [6]. It was recognized that concrete exhibits a critical strain rate called the strain rate threshold above which significant increases in the apparent strength are observed. This apparent strain-rate threshold is nearly equal to $1s^{-1}$ for tension and $60s^{-1}$ for compression in concrete.

In the present analysis the strain rate calculated is of order $10^{-2}s^{-1}$ which it is not a significant value. From the study of Tedesco et.al [6] the DIF values are ~ 1.2 and 1.7 for concrete in compression and tension respectively and an analysis is carried out using DIF value for concrete in compression as well as in tension. As a result, no significant change is observed in the output of numerical simulation and hence it is concluded that strain rate influence is not significant for this problem due to the associated low / moderate strain rate.

NUMERICAL SIMULATION RESULTS AND DISCUSSION

After illustrating the superiority of the fracture energy softening model, the three dimensional finite element numerical simulations of different reinforced concrete slabs tested by Zineddin and Krauthammer [1] were performed to study the effect of impact load. The transient dynamic numerical study of total twelve cases (three drop heights × two reinforcement patterns × two softening models) is carried out for the simulation of experimental tests. The displacement results using the limiting strain and fracture energy based approaches for post cracking softening models are computed and compared with the experimental values as given in Table 3. It is observed that the computed results are consistently in agreement with the reported experimental results with fracture energy based softening model, for simulating the concrete softening behavior. In view of the fact that the strain based softening model gives inconsistent results due to mesh sensitivity effect, further discussions are limited on the results obtained from fracture energy softening model only.

Table 3- Displacement Comparison for Different Slab Tests

Cases	A-1 mesh	B-1 mesh	C-1 mesh	A-2 mesh	B-2 mesh	C-2 mesh
Experimental – Displacement mm(in)	66 (2.6)	102 (4.02)	102 (4.02)	42 (1.65)	71 (2.8)	102 (4.02)
Strain based-Computed Displacement mm(in)	96 (3.77)	68 (2.67)	35 (1.37)	55 (2.16)	66 (2.6)	47 (1.85)
Fracture Energy based – Computed Displacement mm(in)	65 (2.56)	101 (4)	114 (4.5)	41 (1.61)	74 (2.9)	108 (4.25)

Identification of Punching Shear & Flexural Failures

The failure modes such as bending, punching shear and the intermediate mixed mode where the bending failure becomes dominant at the early stages of loading, followed by a transition into punching shear failure mode can be predicted using deformed shape of the slab as given in the study of Miyamoto et.al [7]. The smooth curve with gradual surface and parabolic shape indicate the bending failure. The punching shear failure mode is highly localized near the impact and it appears with negligible amount of deformation along the rest of the slab span with a noticeable inflection point in between the two regions. Therefore in this case the local failure occurs only where the middle portion of the slab is severely affected. At times there are mixed bending and shear failure modes that can appear in the slab, which can be identified through a systematic numerical investigation. Another criteria used in the present study to identify the bending and shear failure modes is based on the flexure/shear stress distribution along the slab span. For the drop height of 152mm, in case of A-2mesh the predominant deformation mode is

flexural while for the case A-1mesh the mixed failure mode is obtained as reported in the experiment by Zineddin and Krauthammer [1]. In case of drop height of 610 mm for case C-2mesh & C-1mesh, the predominant deformation mode is shear punching and for case B-2mesh & B-1mesh with drop height of 305 mm, the mixed failure mode is obtained as reported in the experiment by Zineddin and Krauthammer [1]. From the Figure 2 (c) & 3(c) it is observed that in C-2mesh and C-1mesh the deflected profile is not smooth and the localized effect of punching is observed at the centre of the slab indicating the shear failure. Also the deflection along rest of slab span is negligible and the inflection point is observed so C-2mesh and C-1mesh undergo the punching shear failure. Fig 2 (b) & 3 (b) explain the mixed mode failure in case of B-2mesh and B-1mesh. Firstly the deflected shape is parabolic showing the flexural failure and later the centre of the slab gets severely affected with negligible deflection along rest of the slab span showing the shear failure. In case of A-2mesh, the smooth parabolic profile of displacement is obtained as presented in Fig 2 (a) and during the later stage although the inflection point appears but the central portion of the slab is not affected significantly as flexural behavior of slab is found to be dominant. Similarly in the case A-1mesh the inflection point appears at the later stages and also the parabolic deflected shape of slab is observed at an early stage as is clear from the Figure 3 (a), hence it is concluded that A-1mesh undergo mixed mode of failure. The progressive deflected shapes of slabs A-2mesh and C-1mesh due to central impact as traced with the present numerical simulation are shown along in Figs. 4 & 5 respectively. From the Fig. 4 and Fig. 5, it is clear that A-2mesh shows the predominantly flexural failure and C-1mesh undergoes punching shear failure.

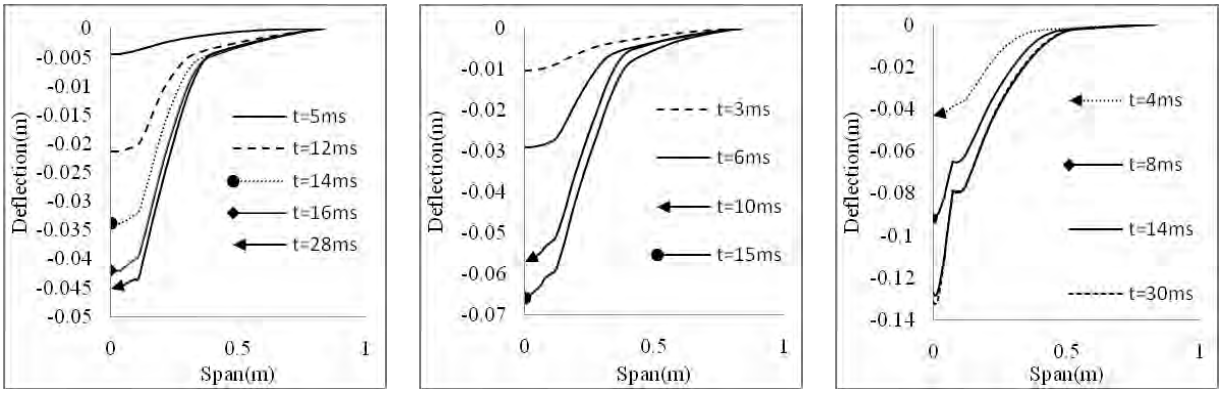

(a) (b) (c)

Figure 2 Deflected slab profile at various time (a) A-2mesh (b) B-2mesh (c) C-2mesh

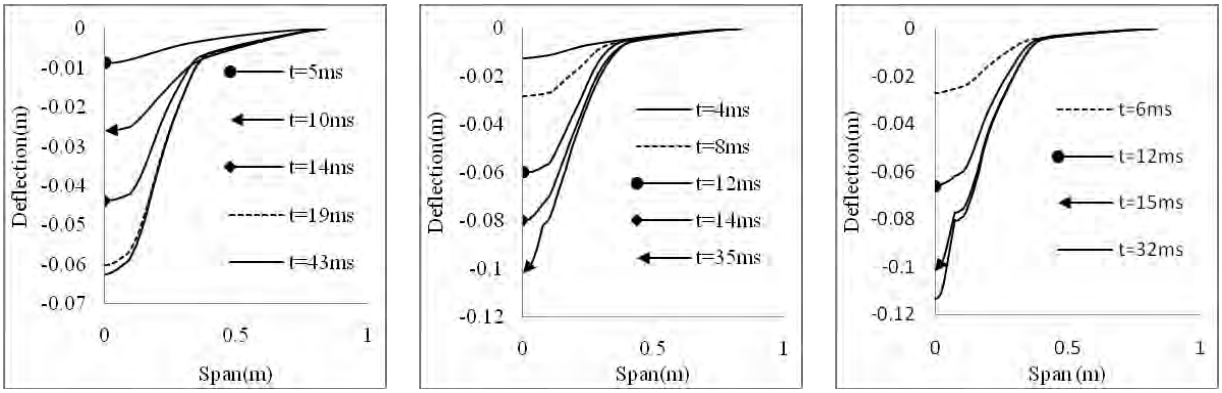

(a) (b) (c)

Figure 3 Deflected slab profile at various time (a) A-1mesh (b) B-1mesh (c) C-1mesh

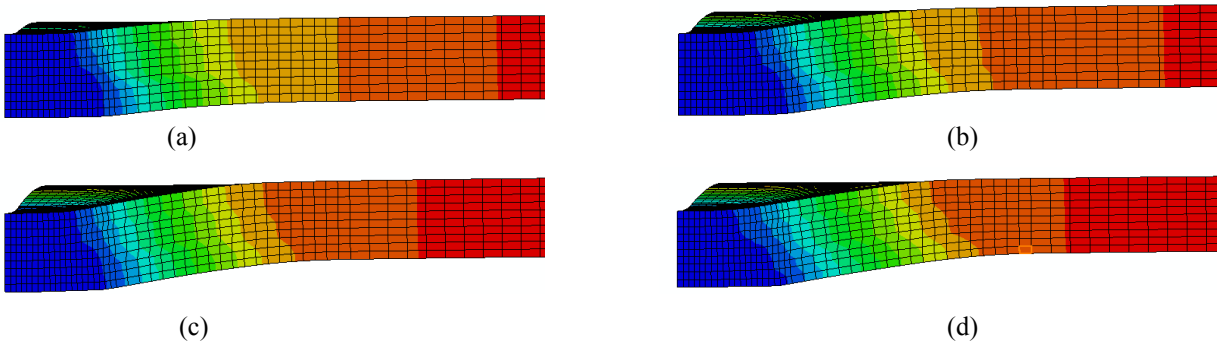

Fig 4 Deflected slab profile of A-2mesh (a) t=12 ms (b) t=14 ms (c) t=16 ms (d) t=28 ms

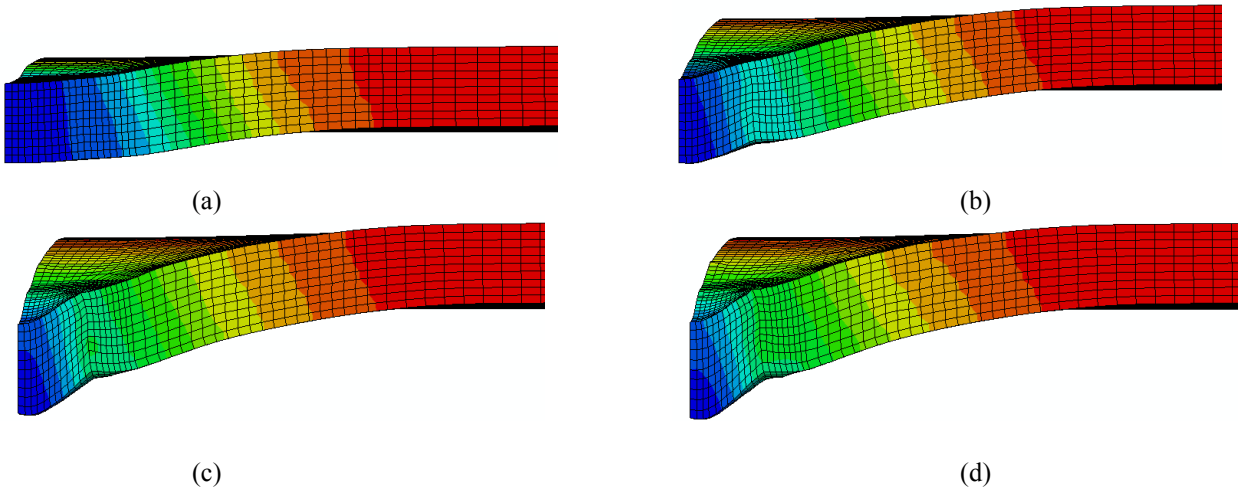

Fig 5 Deflected slab profile of C-1mesh (a) t=6.48 ms (b) t=12.96 ms (c) t=16.2 ms (d) t=34 ms

Detail Evaluation of Crushing & Cracking

The failure behavior of concrete such as crushing and cracking is studied with the help of biaxial failure criteria using the Kupfer curve as available in literature by Tao & V. Phillips [8]. Total six elements are selected and the plots of damage and stresses versus time are obtained. The two elements in the centre along the depth of slab i.e. 90 mm (3.54 in) are designated as centre top and centre bottom. Similarly the element in XZ and YZ plane along the depth of slab i.e. 90 mm (3.54 in) are designated as XZ-top, XZ-bottom, YZ-top, and YZ-bottom respectively. The s_{11} and s_{22} are the stress corresponding to YZ plane and XZ plane respectiveliy.

From the Fig. 6 (a) the crushing of centre top element in ***A-2mesh*** case is seen since the value of s_{11}/f_c' and lies in the third quadrant ***outside*** the Kupfer curve. The same pattern for s_{22}/f_c' is obtained . From the Fig. 6 (b) it is clear that the centre bottom element lies ***inside*** the first and the third quadrant. Here the concrete reaches to its tensile strength, hence crack formation takes place at slab bottom and after that concrete undergoes high compression (inside third quadrant). From the Fig 7 (a) values of s_{11}/f_c' is shown in the third quadrant ***inside*** the Kupfer curve indicating the compression of concrete in XZ plane of the top element. Fig. 7 (b) describe that the bottom element (XZ plane) lies ***inside*** the first quadrant (reaching to tensile strength) where the cracking begins initially and finally it is ***inside*** third quadrant indicating compressive failure. From the Fig. 8 (a) it is noticed that the value of s_{11}/f_c' lies in the third quadrant ***outside*** the Kupfer curve which indicates the crushing of concrete for top element (YZ plane) which is relatively less severe as compared to centre top element. Fig. 8 (b) indicates that bottom element (YZ plane) lies ***inside*** the first quadrant (just reaching to tensile strength) where crack formation starts then subsequently it lies ***inside*** third quadrant due to compression. Like wise the stress study for all other cases are carried. It is concluded from the stress pattern that tensile strength of concrete is attained in ***A-2mesh*** as a result the crack initiation occurs which is controlled since steel-mesh is at the concrete cover of 25 mm (0.984 in) and further the slab undergoes the flexure action, so ***A-2mesh*** is flexure dominant. In the case of ***B-2mesh*** also

reaches to the close value of tensile strength so some cracks may appear. Also the impact load in ***B-2mesh*** is higher than the ***A-2mesh*** so the flexure failure is not that significant and shear failure becomes dominant as a result ***B-2mesh*** undergoes mixed mode of failure. In case of ***C-2mesh***, all the element which are taken into consideration, do not reach to the tensile strength of concrete. Due to a very high value of impact load it is concluded that the failure in case of ***C-2mesh*** is predominantly due to shear punching action. ***A-1mesh***, ***B-1mesh*** and ***C-1mesh*** reaches the tensile strength of concrete so the cracks initiates and further grow due to presence of steel mesh at the centre of slab at concrete cover of 45 mm (1.77 in). Since the impact load in ***A-1mesh*** and ***B-1mesh*** is less than the ***C-1mesh*** , hence ***A-1mesh*** and ***B-1mesh*** first undergo the flexure action and subsequently it undergo the shear failure.

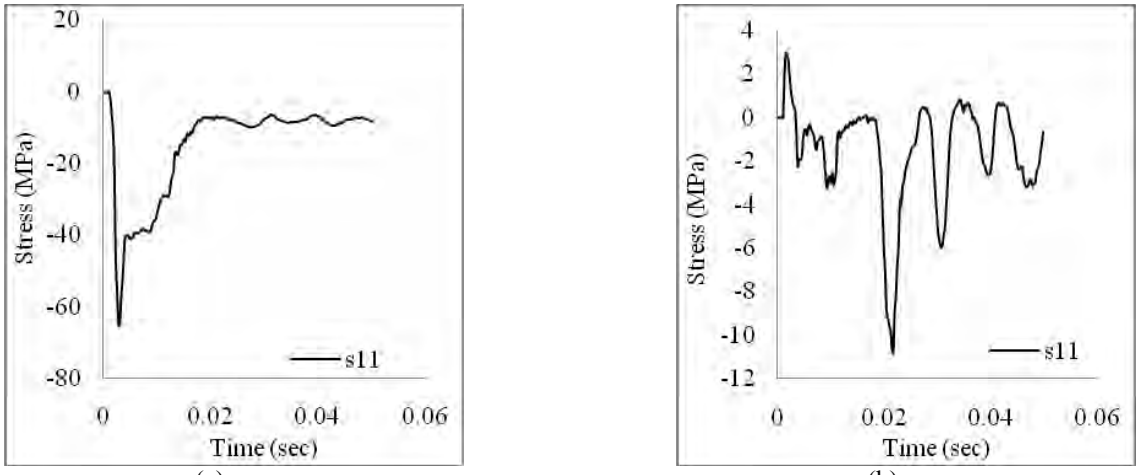

(a) (b)

Fig.6 Stress on (a) top & (b) bottom element at centre in case of A-2mesh

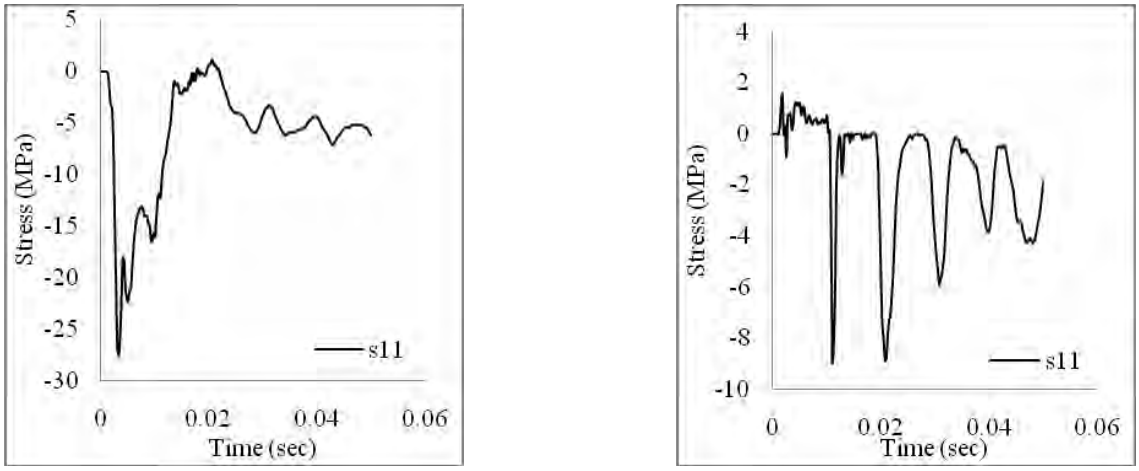

(a) (b)

Fig. 8 Stress on (a) top & (b) bottom element at XZ plane in case of A-2mesh

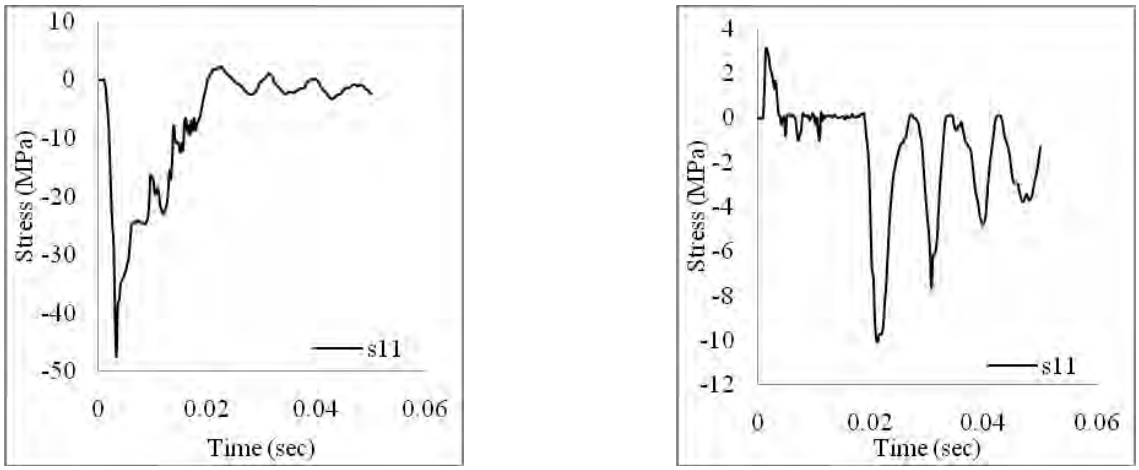

(a) (b)

Fig. 10 Stress on (a) top & (b) bottom element at YZ plane in case of A-2mesh

CONCLUSION

This paper presented a three dimensional finite element model of reinforced concrete slab subjected to drop hammer weight. Numerical simulations have been performed to study the transient dynamic behavior of slab. The deflected profile, stresses and the failure modes of slab due to bending failure, mixed and punching shear failure are studied. The numerical value of deflection is found to be in good agreement with the reported experimental results. The punching shear failure is predicted by observing the inflection point, local failure at the centre of slab and the negligible displacement along the rest of the slab span. The flexural failure is predicted by obtaining the smooth deflected slab profile. The stress variation with time is studied with the help of biaxial failure criteria using the Kupfer curve as available in paper by Tao & V. Phillips [8] where the crushing, cracking, and the influence of stress-biaxiality are systematically accounted. Also the influence of strain rate has been examined using dynamic increase factor (DIF) reported by Tedesco et.al [6] and is shown to be insignificant for the present problem. However, it is possible to simulate the realistic impact behavior of reinforced concrete slabs through a systematic numerical procedure, which accounts for the fracture energy based softening model with due consideration to various failure modes.

REFERENCES

[1] Zineddin M. and Krauthammer T., "Dynamic response and behavior of reinforced concrete slabs under impact loading,". *International Journal of Impact Engineering*, Vol.34, 2007, pp. 1517-1534.
[2] Bazant Z. P and Planas J., "Fracture and Size Effect in Concrete and other Quasibrittle Materials," *CRC Press*, Florida, 1998.
[3] Singh R K, Basha S M, and Singh Rajesh K., "Fracture Energy and Size Effect Studies for Nuclear Concrete Structures," Proc. SMiRT-20, Espoo, Espoo, Finland, August 9-14, 2009
[4] ABAQUS analysis user's manual, *Version 6.8*.
[5] Mehta P Kumar and Monteiro Taulo J M., "Concrete Microstructure Property and Materials," 1997.
[6] Tedesco J. W., Powell J. C., Ross Allen and Hughes M. L., "A strain rate dependent concrete material model for Adina," *Computers & Structures*, V.64, 1997, pp. 1053-1067.
[7] Miyamoto Ayaho, W. King Michael, Fujii Mamabu. Analysis of Failure Modes for Reinforced Concrete Slabs under Impulsive Loads. ACI Structure Journal. 1991;88.
[8] Tao Xiaoya and V. Phillips David., "A simplified isotropic damage model for concrete under bi-axial stress states," *Cement and Concrete composites*, 2004.